



1st International Conference on the Material Point Method, MPM 2017

Projection method in material point method for modeling incompressible materials

Shyamini Kularathna^{a,*}, Kenichi Soga^b

^a*Department of Engineering, Geotechnical and Environmental Research Group, University of Cambridge, CB2 1PZ, United Kingdom*

^b*Department of Civil and Environmental Engineering, University of California Berkeley, Berkeley 94720, USA*

Abstract

Material point method is a variant of the finite element method (FEM) and is successfully applied in large deformation problems. Recently, material point method has been applied in a wide range of engineering applications including solid and solid-fluid interaction problems. However, describing the behavior of incompressible materials is a challenging problem in MPM. The explicit formulation and the linear elements used in the standard MPM exhibit numerical instabilities such as mesh locking and artificial pressure oscillations in material incompressibility. Further, the small time step used to obtain a reasonable numerical stability limits the application of MPM in problems particularly with long time durations. We present an implicit treatment of the pressure term in MPM to mitigate the numerical instabilities and small time steps in incompressible material problems. The set of velocity-pressure coupled governing equations resulted by the implicit formulation is solved using Choin's projection method. The numerical examples show that the present MPM implementation is capable of modeling incompressible materials without pressure oscillations using a significantly large time step.

© 2016 The Authors. Published by Elsevier Ltd.

Peer-review under responsibility of the organizing committee of the 1st International Conference on the Material Point Method.

Keywords: material point method; incompressible materials; projection method.

1. Introduction

Material point method (MPM) which is categorized as a particle based method was first developed for solid mechanics problems with history dependent materials and large deformations. Recently, MPM has been used in many engineering applications including solid and solid-fluid interaction problems.

* Corresponding author.

E-mail address: srhgk2@cam.ac.uk

However, the standard explicit formulation and the linear elements used in MPM lead to artificial pressure oscillations and significantly small time steps in incompressible and near incompressible material problems. The common approach to obtain a reasonable stable solution to the material incompressibility is to use enhanced strain values for pressure calculation [1,2]. Even though these enhancing techniques improve the pressure calculation, the standard explicit MPM still experiences small time steps and numerical instabilities particularly in complex material behaviors with a strong dependency on the pressure. The aim of our work is to present an improved MPM formulation for modeling incompressible materials.

We implement an implicit treatment of the pressure within MPM to model incompressible materials. Chorin's projection method is used to solve the velocity-pressure coupled governing equations resulted by the implicit formulation. Projection method was originally introduced by [3] to solve incompressible Navier-stokes equations in fluid mechanics applications. Later, the projection method has been extensively used in both mesh based methods [4, 5] and particle based methods [6, 7] to solve incompressible fluids. The use of the projection method in MPM is comparatively new. The work by [8] presents successful application of the Chorin's projection method in MPM to model arbitrarily incompressible and phase changing materials. In this paper, we study the effectiveness of the Chorin's projection method in MPM with linear quadrilateral elements for fully incompressible materials.

2. Formulation of MPM for incompressible materials

2.1. Governing equations

Let $\rho(\mathbf{x},t)$ be the density, $\mathbf{v}(\mathbf{x},t)$ be the velocity, $\boldsymbol{\sigma}(\mathbf{x},t)$ be the Cauchy stress tensor and $\mathbf{b}(\mathbf{x},t)$ be the body force of the material point in its current configuration. Neglecting thermal effects, the motion of the continuum body is governed by the conservation of mass, conservation of momentum and constitutive equations. Applying the incompressible condition and splitting the Cauchy stress tensor in to dilational part, p and deviatoric part, $\boldsymbol{\tau}$, the governing equations can be written in the following implicit form.

$$\rho \frac{\mathbf{v}^{t+1} - \mathbf{v}^t}{\Delta t} = -\nabla p^{t+1} + \nabla \cdot \boldsymbol{\tau} + \rho \mathbf{b} \quad (1)$$

$$\nabla \cdot \mathbf{v}^{t+1} = 0 \quad (2)$$

$$\mathbf{v}^{t+1} = \mathbf{v}_b \text{ on } \partial\Omega_D \quad (3)$$

where $\partial\Omega_D$ is the Dirichlet boundary surface.

The coupled equations (1) and (2) are solved using the Chorin's projection method. In this technique, equation (1) is split into two equations (Eqs. (4) and (5)) introducing an intermediate velocity, \mathbf{v}^* with appropriate boundary conditions (Eq. (6)).

$$\rho \frac{\mathbf{v}^* - \mathbf{v}^t}{\Delta t} = \nabla \cdot \boldsymbol{\tau} + \rho \mathbf{b} \quad (4)$$

$$\rho \frac{\mathbf{v}^{t+1} - \mathbf{v}^*}{\Delta t} = -\nabla p^{t+1} \quad (5)$$

$$\mathbf{v}^* = \mathbf{v}_b^* \text{ on } \partial\Omega_D \quad (6)$$

The implicit pressure term is solved by taking the divergence of equation (5) and substituting equation (2) in order to eliminate $\nabla \cdot \mathbf{v}^{t+1}$. This results in an elliptic equation as

$$\nabla^2 p^{t+1} = \frac{\rho}{\Delta t} \nabla \cdot \mathbf{v}^* \quad (7)$$

2.2. Weak formulation and numerical integration

The computational algorithm includes three main steps (i) solving intermediate velocity field using equation (4) (ii) solving the elliptic equation (7) for implicit pressure and (iii) updating the velocity using equation (5). The weak forms of the governing equations are obtained by multiplying the equations (4), (5) and (7) by appropriate test functions.

Deviating from the standard material point based integration in MPM, we employ Gaussian integration points for the elements densely filled with material points and the usual summation over the material points for partially filled elements. This approach helps mitigating any numerical instability caused by the matrices with randomly positioned material points. The elements are identified as fully filled or partially filled using the ratio (θ) between the summation of the volume of material points in an element and the volume of that particular element. We use the ratio above 0.9 to define the fully (Eq.(8)) and partially (Eq.(9)) filled elements in our study. Furthermore, the elements with the ratio below 0.2 were omitted from the integration in order to avoid ill conditioned matrices resulting from nodes with nearly zero masses.

$$\frac{\sum_{p=1}^{N_p^e} V_p}{V_e} \geq 0.9 \text{ for fully filled elements} \quad (8)$$

$$\frac{\sum_{p=1}^{N_p^e} V_p}{V_e} < 0.9 \text{ for partially filled elements} \quad (9)$$

where V_p is the volume of the material point, V_e is the volume of the considered element and N_p^e is the number of particles in the element.

In solving equation (4), the body force, \mathbf{b} and the traction forces, \mathbf{t} are discretised at material points similar to the standard MPM implementation. To demonstrate the performance of the proposed method, we present numerical examples of viscous free incompressible fluid flow in this paper for simplicity. This leads to the following usual equations (Eqs. (10) and (11)) to be solved. The intermediate velocity is then solved using equation (12).

$$M_i \mathbf{a}_i^* = \mathbf{f}_i^{ext} \quad (10)$$

$$\mathbf{f}_i^{ext} = \sum_{p=1}^{N_p} m_p N_i(\mathbf{x}_p) \mathbf{b}_p + \oint N_i(\mathbf{x}) \mathbf{t} dS \quad (11)$$

$$\mathbf{v}_i^* = \mathbf{v}_i^t + \Delta t \mathbf{a}_i^* \quad (12)$$

where N_i is the nodal shape function for velocity, M_i is the lumped mass at i^{th} node, \mathbf{a}_i^* is an intermediate acceleration term at i^{th} node, \mathbf{f}_i^{ext} is the external force at i^{th} node and m_p is the mass of the material point at \mathbf{x}_p .

Applying the numerical integration appropriately and taking the homogeneous Neumann pressure boundary condition $\nabla p^{t+1} \cdot \mathbf{n}$ to be zero, the elliptic equation (7) for the implicit pressure can be written in the following matrix form.

$$[L]\{\mathbf{p}^{t+1}\} = -\frac{\rho}{\Delta t}[D]\{\mathbf{v}^*\} \quad (13)$$

$$[L] = \sum_{i,j=1}^{n_n^p} \left\{ \sum_{n=1}^{n_n^v} \omega_n \nabla N_i^p(\mathbf{x}_n) \nabla N_j^p(\mathbf{x}_n) \right\} \quad (14)$$

$$[D] = \sum_{i=1}^{n_n^p} \sum_{j=1}^{n_n^v} \left\{ \sum_{n=1}^{N_{qp}} \omega_n N_i^p(\mathbf{x}_n) \nabla N_j(\mathbf{x}_n) \right\} \quad (15)$$

where n_n^p is the number of nodes where pressure is solved, n_n^v is the number of nodes where velocity is solved, n_{qp} is the number of integration points, \mathbf{x}_n and ω_n is the weight of the integration point, \mathbf{x}_n . N_i^p is the nodal basis function

for pressure.

Finally, applying the numerical integration over the Gaussian quadrature points and the material points, the velocity update equation (5) can be written as

$$[M]\{\mathbf{v}^{t+1}\} = [M]\{\mathbf{v}^*\} - \frac{\Delta t}{\rho} [G]\{p^{t+1}\} \quad (16)$$

$$[M] = \sum_{i,j=1}^{n_p^p} \left\{ \sum_{n=1}^{N_{qp}} \omega_n N_i(\mathbf{x}_n) N_j(\mathbf{x}_n) \right\} \quad (17)$$

$$[G] = \sum_{i=1}^{n_p^p} \sum_{j=1}^{n_p^p} \left\{ \sum_{n=1}^{N_{qp}} \omega_n N_i(\mathbf{x}_n) \nabla N_j^p(\mathbf{x}_n) \right\} \quad (18)$$

The particle velocity, pressure and position are updated using the nodal values as in equations (19), (20) and (21).

$$\mathbf{v}_p^{t+1} = \mathbf{v}_p^t + \sum_{i=1}^{n_n} N_i(\mathbf{x}_p^t) (\mathbf{v}_i^{t+1} - \mathbf{v}_i^t) \quad (19)$$

$$\rho_p^{t+1} = \sum_{i=1}^{n_n} N_i(\mathbf{x}_p^t) \rho_i^{t+1} \quad (20)$$

$$\mathbf{x}_p^{t+1} = \mathbf{x}_p^t + \Delta t \sum_{i=1}^{n_n} N_i(\mathbf{x}_p^t) \mathbf{v}_i^{t+1} \quad (21)$$

3. Numerical examples

The dam break problem without an obstacle at the bottom was analyzed using the present MPM algorithm. The mesh sensitivity, time step and numerical stability of the implicit MPM formulation were compared with those of the explicit MPM in which the pressure was evaluated at the center of 4-node quadrilateral element and additional pressure smoothing was applied. In the present MPM analysis, water was considered to be viscous free and the density of water was taken as 1000 kg/m^3 . The bulk modulus (K) of water was assumed to be 2.2 GPa in the explicit MPM analysis.

The model parameters used in the explicit and the implicit simulations are given in Table 1. The total computational domain (see Fig. 1) of $0.42 \text{ m} \times 0.44 \text{ m}$ was represented by three different meshes. The water column was modeled using 16 particles per cell. In the implicit MPM simulations, the initial pressure of the material points was set to zero. It should also be noted that applying the hydrostatic pressure to the material points as the initial pressure had no effect on the simulation. At each time step, the grid nodes which correspond to the free surface of the water column were identified in both simulations and the free surface boundary condition was applied.

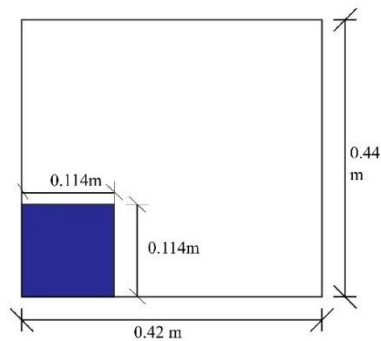


Fig. 1. Dam break without an obstacle at the bottom: MPM model.

Table 1. MPM model parameters for dam break problem.

Mesh spacing	0.0114m		0.008m		0.004m	
Particle spacing	0.00285m		0.002m		0.001m	
K (GPa)	2.2	N/A	2.2	N/A	2.2	N/A
Δt (s)	1×10^{-6}	1×10^{-2}	1×10^{-7}	1×10^{-3}	1×10^{-7}	1×10^{-3}
Total time (s)	1.00	1.00	1.00	1.00	1.00	1.00
	Explicit	Implicit	Explicit	Implicit	Explicit	Implicit

As shown in Table 1, the time step used in the implicit MPM is 10,000 times larger compared to the small time step used in the standard fully explicit formulation which was 1×10^{-7} s. The variation of the height (h) and the evolution of the water front (l) of the water column given by the two MPM formulations are compared in Fig. 2(a) and 2(b) for each mesh. The results exhibit a close agreement without any dependency on the mesh size.

Further, the pressure distribution at different instants obtained from the explicit and the implicit MPM analysis using the mesh of 0.004m is compared in Fig. 3. While both simulations present similar pressure variation, the implicit MPM formulation with the projection method shows a smooth pressure distribution. Moreover, in comparison to the turbulent behavior in the explicit calculation, a damping effect can be seen in the implicit MPM simulation towards the end of the total analysis time. This damped behavior of the present implicit calculation can be attributed to the zero pressure gradients caused by neglecting the elements with small number of particles in the system of matrix solution.

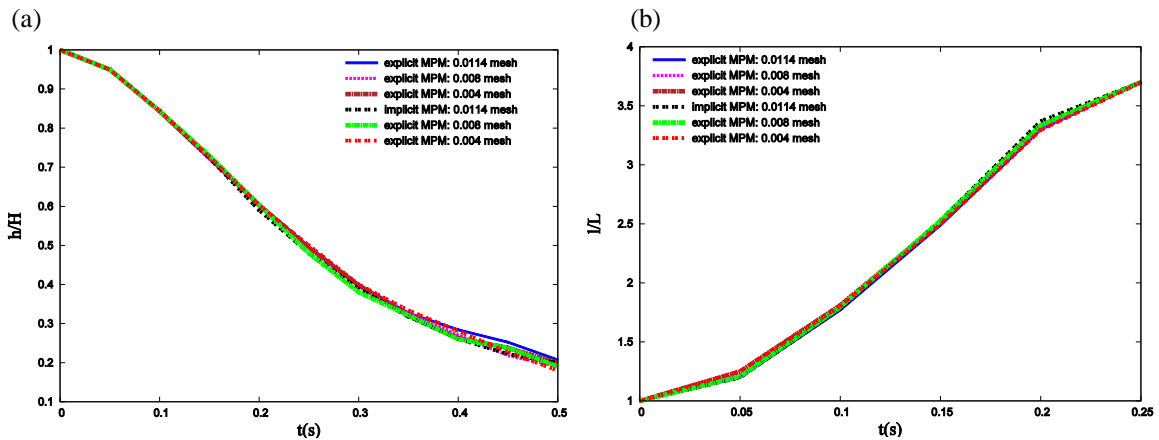


Fig. 2. Comparison of explicit and implicit MPM simulation (a) normalized height of water column with time; (b) normalized length of water front with time.

The results were further compared with the experimental data presented in [9] and the numerical results from the open source software, OpenFoam. As can be seen in Fig.4, the water profile obtained from each analysis and the experiment follows a similar variation. It is worth noting that in Fig. 4(a), 4(b) and (c), the water front in the numerical results is faster than that of the experiment. The assumptions of viscous free water and zero surface tension in the numerical simulations can result in the observed difference of the water front.

Furthermore, a number of isolated material points which has no physical meaning can be seen in both explicit and implicit MPM simulations. This behaviour which is particular to MPM is caused by the spurious velocities of a small number of particles moving through the adjacent grid cells.

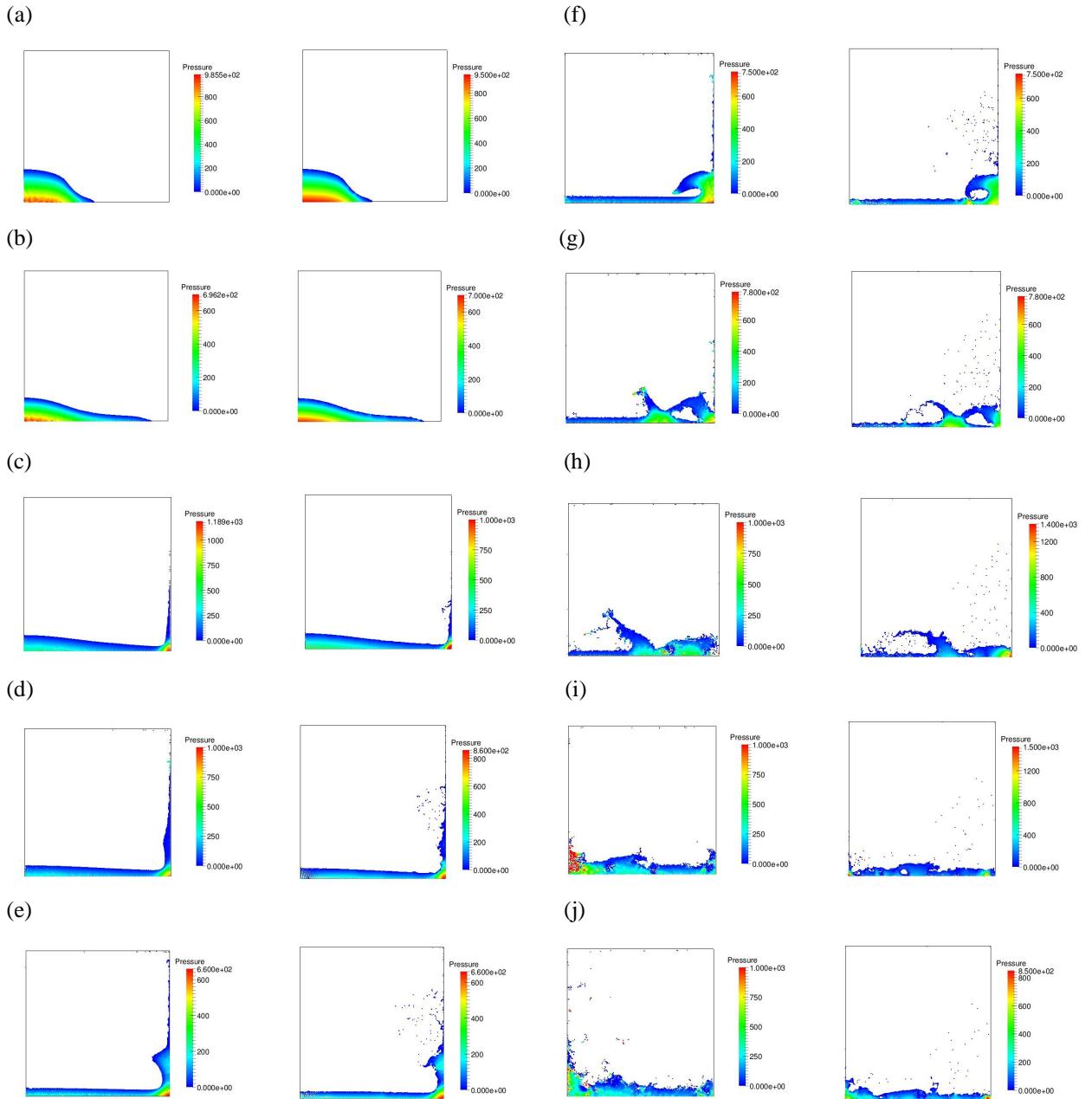


Fig. 3. Pressure distribution: explicit MPM (left) implicit MPM (right) (a) 0.1 s; (b) 0.2 s; (c) 0.3 s; (d) 0.4 s; (e) 0.5 s; (f) 0.6 s; (g) 0.7 s; (h) 0.8 s; (i) 0.9 s; (j) 1.0 s.

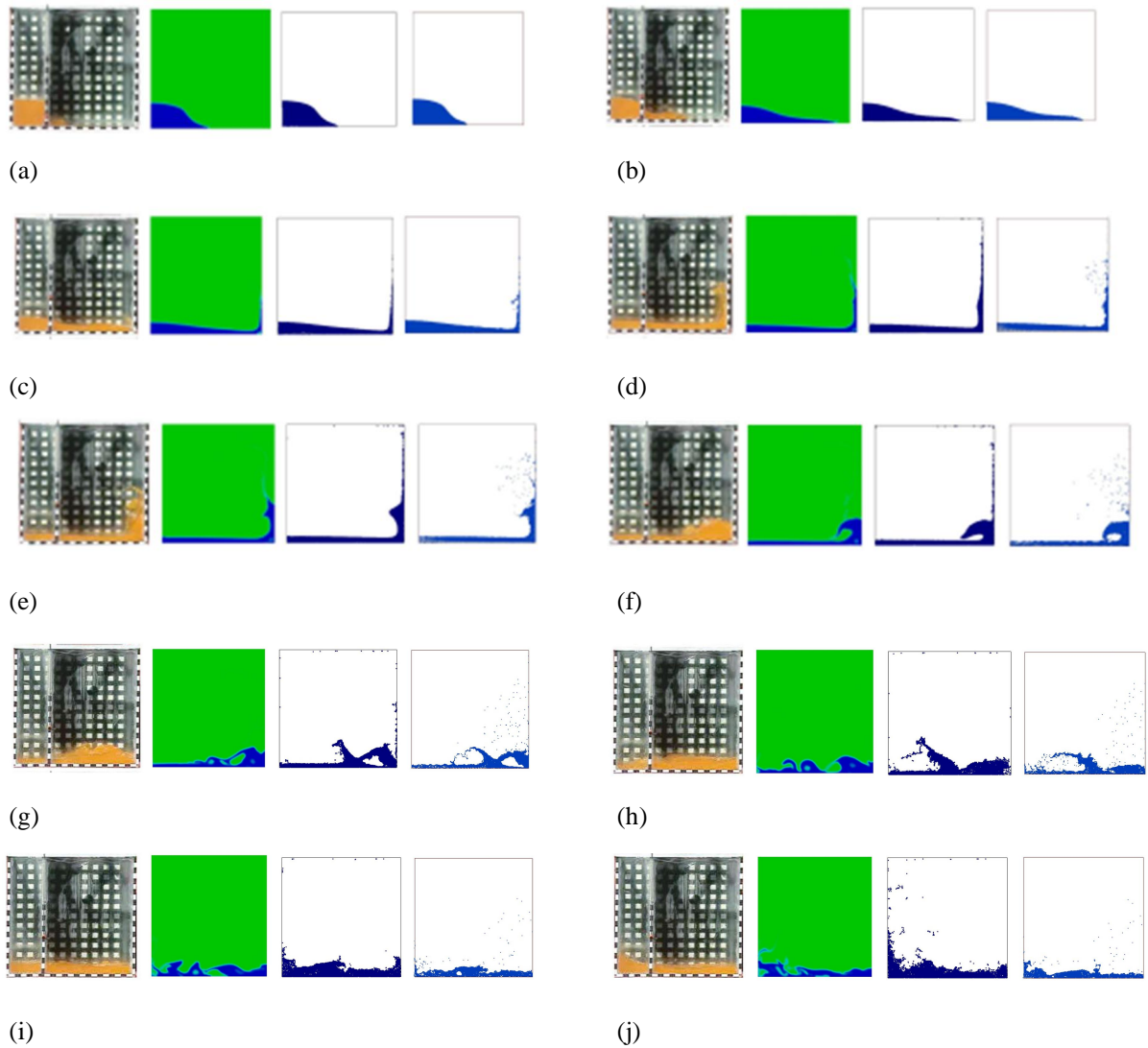


Fig. 4. Comparison of water profile at different instants: (from left to right) experiment, openFoam , explicit MPM using 0.004m mesh and implicit MPM using 0.004m mesh (a) 0.1 s; (b) 0.2 s; (c) 0.3 s; (d) 0.4 s; (e) 0.5 s; (f) 0.6 s; (g) 0.7 s; (h) 0.8 s; (i) 0.9 s; (j) 1.0 s.

4. Conclusions

This paper describes an implicit MPM formulation based on Chorin's projection method for solving incompressible material problems. The close agreement between the results demonstrates the capability of the implicit MPM formulation to solve fully incompressible material problems. Specially, the implicit formulation allows a large time step compared to the significantly small time step in explicit MPM formulation at near incompressible conditions.

Acknowledgements

This study has been financially supported by the Cambridge Commonwealth Trust and the European Unions Seventh Framework Programme 662 for research, technological development and demonstration under grant agreement no PIAP-GA-663 2012-324522 (MPM Dredge).

References

- [1] S. Bandara, K. Soga, Coupling of soil deformation and pore fluid flow using material point method, *Comput. Geotech.* 63 (2015) 199–214.
- [2] F.M. Hamad, Formulation of a dynamic material point method and applications to soil-water-geotextile systems, University of Stuttgart, 2014.
- [3] A.J. Chorin, Numerical Solution of the Navier-Stokes Equations, *Math. Comput.* 22 (1968) 745–762.
- [4] B. Bell, P. Colella, A second-order projection method for the incompressible Navier-Stokes equations, *J. Comput. Phys.* 85 (1989) 257–283.
- [5] J.-L. Guermond, L. Quartapelle, Calculation of Incompressible Viscous Flows by an Unconditionally Stable Projection FEM, *J. Comput. Phys.* 132 (1997) 12–33.
- [6] E. Lee, V. Damient, R. Issa, S. Ploix, Application of weakly compressible and truly incompressible SPH to 3-D water collapse in waterworks, *J. Hydraul. Res.* 48 (2009) 50–60.
- [7] E.S. Lee, C. Moulinec, R. Xu, D. Violeau, D. Laurence, P. Stansby, Comparisons of weakly compressible and truly incompressible algorithms for the SPH mesh free particle method, *J. Comput. Phys.* 227 (2008) 8417–8436.
- [8] A. Stomakhin, C. Schroeder, C. Jiang, L. Chai, J. Teran, A. Selle, Augmented MPM for phase-change and varied materials, *ACM Trans. Graph.* 33 (2014) 1–11.
- [9] M. a. Cruchaga, D.J. Celentano, T.E. Tezduyar, Collapse of a liquid column: numerical simulation and experimental validation, *Comput. Mech.* 39 (2006) 453–476.